FINITE ELEMENT STUDY ON LOCAL BUCKLING AND ENERGY DISSIPATION OF SEISMIC BRACING

A THESIS SUBMITTED TO
THE GRADUATE SCHOOL OF NATURAL AND APPLIED SCIENCES
OF
MIDDLE EAST TECHNICAL UNIVERSITY

BY

AHMET KUŞYILMAZ

IN PARTIAL FULFILLMENT OF THE REQUIREMENTS
FOR
THE DEGREE OF MASTER OF SCIENCE
IN
CIVIL ENGINEERING

JUNE 2008

Approval of the thesis:

FINITE ELEMENT STUDY ON LOCAL BUCKLING AND ENERGY DISSIPATION OF SEISMIC BRACING

submitted by **AHMET KUŞYILMAZ** in partial fulfillment of the requirements for the degree of **Master of Science in Civil Engineering Department, Middle East Technical University** by,

Prof. Dr. Canan Özgen _____
Dean, Graduate School of **Natural and Applied Sciences**

Prof. Dr. Güney Özcebe _____
Head of Department, **Civil Engineering**

Assoc. Prof. Dr. Cem Topkaya _____
Supervisor, **Civil Engineering Dept., METU**

Examining Committee Members:

Prof. Dr. Çetin Yılmaz _____
Civil Engineering Dept., METU

Assoc. Prof. Dr. Cem Topkaya _____
Civil Engineering Dept., METU

Prof. Dr. Mehmet Utku _____
Civil Engineering Dept., METU

Assoc. Prof. Dr. Ahmet Yakut _____
Civil Engineering Dept., METU

Volkan Aydoğan _____
Civil Engineer (M.S.) , PROMA

Date: 27.06.2008

I hereby declare that all information in this document has been obtained and presented in accordance with academic rules and ethical conduct. I also declare that, as required by these rules and conduct, I have fully cited and referenced all material and results that are not original to this work.

Name, Last name : Ahmet KUŞYILMAZ

Signature :

ABSTRACT

FINITE ELEMENT STUDY ON LOCAL BUCKLING AND ENERGY DISSIPATION OF SEISMIC BRACING

Kuşyılmaz, Ahmet
M.S., Department of Civil Engineering
Supervisor: Assoc. Prof. Dr. Cem Topkaya

June 2008, 40 pages

Seismic provisions for steel buildings present limiting width-thickness and slenderness ratios for bracing members. Most of these limits were established based on experimental observations. The number of experimental studies is limited due to the costs associated with them. With the rapid increase in computing power; however, it is now possible to conduct finite element simulation of brace components using personal computers. A finite element study has been undertaken to evaluate the aforementioned limits for pin-ended pipe section steel braces. Fifty four tubular pipe brace models possessing different diameter-to-thickness ratios varying from 5 to 30 and slenderness ratios varying from 40 to 200 were analyzed. The effect of cyclic hardening modulus on the response of braces was explored. In all analysis, the models were subjected to reversed cyclic displacements up to ten times the yield displacement. Local buckling was traced during the loading history using a criterion based on local strains. Results are presented in terms of the ductility level attained by the member at the onset of local buckling. It is shown that local buckling of the section is influenced by the diameter-to-thickness and the slenderness ratios of the member. Moreover, the amount of hardening modulus was found to affect the local buckling response significantly. The need to include this material property

into seismic provisions is demonstrated. Finally, the hysteretic energy dissipated by the member was quantified for each displacement excursion.

Keywords: Bracing, seismic response, local buckling, energy dissipation, finite elements

ÖZ

ÇELİK ÇAPRAZ ELEMANLARDA YEREL BURKULMA VE ENERJİ SÖNÜMÜNÜN SONLU ELEMANLAR METODUYLA İNCELENMESİ

Kuşyılmaz, Ahmet
Yüksek Lisans, İnşaat Mühendisliği Bölümü
Tez Yöneticisi: Doç. Dr. Cem Topkaya

Haziran 2008, 40 sayfa

Çelik yapılar hakkındaki deprem yönetmelikleri genişlik/kalınlık ve narinlik oranları hakkında limit değerler içerir. Bu limit değerlerin çoğu deneysel gözlemler sonucunda belirlenmiştir. Yapılmış olan deneysel çalışmaların sayısı yüksek maliyetleri sebebiyle sınırlıdır. Fakat bilgi işleme gücündeki hızlı artış sayesinde günümüzde çelik çaprazların sonlu elemanlar simülasyonları kişisel bilgisayarlarda yapılabilmektedir. Yönetmeliklerdeki mevcut limitlerin değerlendirilmesi amacıyla mafsallı boru kesit çelik çaprazlar üzerinde sonlu elemanlar analizi içeren bir çalışma yapılmıştır. Çap/kalınlık oranları 5 ila 30, narinlik oranları 40 ila 200 arasında değişen elli dört boru kesit çapraz modeli analiz edilmiştir. Çevrimli pekleşme modülünün çaprazların davranışına olan etkisi incelenmiştir. Bütün analizlerde modellere akma deplasmanlarının on katına kadar ters çevrimli deplasmanlar uygulanmıştır. Yükleme sırasındaki yerel deformasyonlara bağlı bir kriter kullanılarak, yerel burkulma tespit edilmiştir. Elde edilen sonuçlar, elemanların yerel burkulma başlangıcı esnasındaki süneklik dereceleri cinsinden sunulmuştur. Bir elemanın çap/kalınlık ve narinlik oranlarının yerel burkulmayı etkilediği görülmüştür. Ayrıca, pekleşme modülü değerinin yerel burkulma davranışı üzerinde ciddi etkisinin olduğu anlaşılmıştır.

Bu malzeme özelliğinin deprem yönetmeliğindeki sınırlandırmalara dahil edilmesi gereği görülmüştür. Son olarak, elemanın her deplasman döngüsü için sönümlediği çevrimsel enerji miktarı bulunmuştur.

Anahtar sözcükler: Çaprazlama, sismik performans, yerel burkulma, enerji sönümleme, sonlu elemanlar

ACKNOWLEDGMENTS

This study was performed under the supervision of Dr. Cem Topkaya. I would like to express my sincere appreciation for his invaluable support, guidance and insights throughout my study.

I would like to express my deepest thanks to Mustafa Can Yücel for his encouragements, productive comments and invaluable discussions throughout this study.

This study was supported by a contract from The Scientific & Technological Research Council of Turkey (TÜBİTAK – 105M242). Also, the scholarship provided by TÜBİTAK during my graduate study is highly acknowledged.

I would like to express my deepest appreciation to my parents for the support, friendship, and understanding that they have provided for me throughout my life.

TABLE OF CONTENTS

PAGE

LIST OF TABLES

TABLES

LIST OF FIGURES

FIGURES

CHAPTER 1

INTRODUCTION

1.1 Background

Steel braced frames are widely used as a lateral load resisting system and it is highly useful in absorbing and dissipating earthquake energy. In concentrically braced frames energy is dissipated through yielding and post-buckling hysteresis behavior of bracing members upon cyclic loading. Requirements for ductility and energy dissipation capability of brace members have been added to the design specifications over the years. In order to ensure the desired behavior, the slenderness and width-thickness ratios of these members are limited by the specifications.

During a moderate to severe earthquake, bracing members that are subjected to compressive forces will buckle and contribute to energy dissipation. The braces could undergo post-buckling axial deformations 10 to 20 times their yield deformation (AISC Commentary 2005). Design requirements are based on the premise that bracing members with low slenderness ratio (KL/r) have superior seismic performance. For diagonal brace members the following slenderness ratio limits are given in AISC Seismic Provisions (2005) and Eurocode 8:

Bracing members shall have $KL/r \leq 4\ E/F_y$

where

K = Effective length factor

L = Length of the truss member

r = Governing radius of gyration

E = Modulus of elasticity of steel (200,000 MPa)

F_y = Specified minimum yield stress of the type of steel to be used

(AISC 2005) (1.1)

In AISC 2005 slenderness ratios up to 200 are allowed but there are special requirements for systems with such high slenderness values.

In Eurocode 8 for frames with X diagonal bracings, slenderness should be limited to: $4.08\sqrt{\frac{E}{F_y}} < KL/r \leq 6.28\sqrt{\frac{E}{F_y}}$ (EUROCODE 8) (1.2.)

The design philosophy was that braces with low slenderness value can significantly contribute to energy dissipation while maintaining a reasonable level of compressive strength.

A plastic hinge forms at the brace midpoint when the member buckles. The plastic hinge region is prone to local buckling. Local buckling can cause high localized strains which eventually trigger low cycle fatigue and may result in fracture of the member during repeated inelastic cycles. Therefore, local buckling leading to fracture may represent a limitation on performance. Fracture developing after local buckling is particularly important for hollow structural section (HSS) brace members (Hassan and Goel 1991; Tang and Goel, 1989; Tremblay 2002). A representative model for local buckling at the mid-length of the brace is given in Figure 1.1.

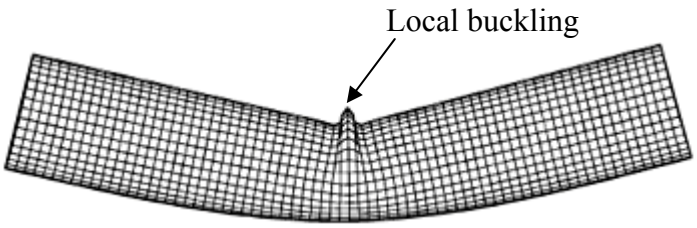

Figure 1.1 : Local Buckling in Brace Model

In order to forestall local buckling, design recommendations (AISC Seismic Provision 2005; Eurocode 3) provide limits on width-thickness ratios of compression elements. For round HSS (pipe section) brace members the following limits are given in AISC Seismic Provisions and Eurocode 3:

$$\frac{D}{t} \le 0.044 \frac{E}{F_y} \qquad \text{(AISC 2005)} \qquad (1.3)$$

$$\frac{D}{t} \le 0.059 \frac{E}{F_y} \qquad \text{(EUROCODE 3 for Class 1 sections)} \qquad (1.4)$$

where D: diameter of the brace; t: wall thickness

1.2 Previous Studies

1.2.1 Experimental Studies

1.2.1.1 Study of Black, Wenger, Popov (1980)

This research experimentally evaluates the hysteretic behavior of axially loaded steel struts. A total of twenty-four specimens were subjected to cyclic quasi-statically applied axial loads simulating earthquake effects. The structural shapes tested were wide-flanges, double-angles, double-channels, and both thick and thin round and square tubes. The material for all rolled sections conformed to ASTM specifications for A36 steel; for pipes, to A53 Grade B steel; for square tubes to A501 steel. Eighteen of the specimen were pinned at both ends and had slenderness ratios of 40, 80, 120; the remaining six specimens, pinned at one end and fixed at the other, had slenderness ratios of 40 and 80.

There are three specimens for pipe sections having the boundary conditions as pinned at both ends, named as Strut 14, 15 and 16. Strut 14 is a 4 inch diameter standard pipe as described in AISC specifications, having a length

of 3.07 m and a slenderness ratio 80. Strut 15 is stated to be physically identical to Strut 14. The difference between Strut 14 and 15 is in the initial loading cases, as Strut 15 was subjected to initial tension load before compression loading in order to compare the effect of loading histories to the buckling behavior of struts. For the specimens Strut 14 and 16, the initial loading was given as compression. Strut 16 is a 4 inch diameter extra strong pipe as described in AISC specifications, having a length of 3.01m and a slenderness ratio of 80.

The results of this experimental research were compared with conventional design procedures for axially loaded members based on AISC specifications. Also, some suggestions for analytic predictions of weakening capacity of struts due to severe cyclic loading were proposed.

1.2.1.2 Study of Zayas, Popov and Mahin (1980)

In this research program six tubular steel braces were tested. The objectives of their study were to present the experimental data in a form which can later be utilized in analytical studies, and to interpret the experimental observations. The findings of this study are used as a benchmark in this thesis because local buckling was observed in the experiments and its occurrence is well documented.

The specimens tested by Zayas et al. (1980) were one-sixth scale models of bracing members used in offshore structures. All specimens had a diameter of 102 mm. The specimens had either 2.1 mm or 3.1 mm wall thickness which resulted in a diameter-to-thickness ratio of 48 and 33, respectively. Of the six specimens, four had pinned ends while the other two had fixed ends. For the pin-ended specimens the length of structural tubing was 1407 mm. All specimens were made of AISI 1020 mild steel tubing which is similar in carbon content and properties to ASTM A36 steel. Because of the drawing process used in its manufacture, the material properties of this tubing in the as-received condition are

considerably different from the A36 steel. Four of the specimens were annealed by heating and oven cooling to obtain material properties that are similar to the one of A36 steel.

All specimens were subjected to quasi-static cycles of reversing axial displacement. These cycles included compressive inelastic buckling followed by tensile stretching. In a typical experiment applied load, axial and lateral displacements and strains at certain critical points were recorded. The test layout used for this study is illustrated in Figure 1.2.

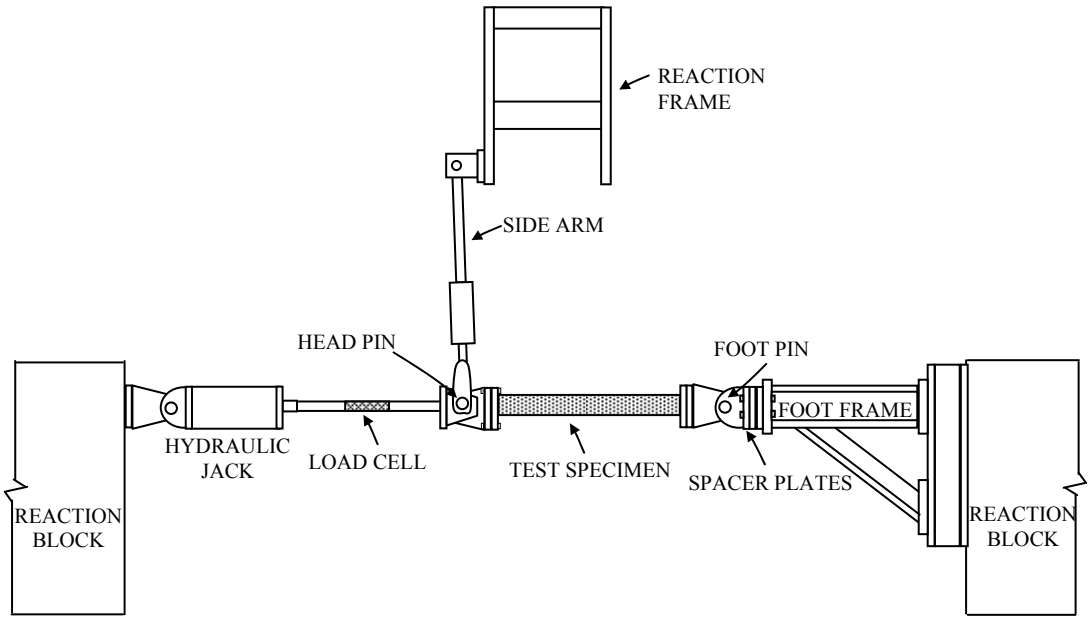

Figure 1.2 : Test Layout for Zayas et al. (1980)

As a part of this thesis, finite element models were developed for the specimens Strut 1 and Strut 2 which had a diameter-to-thickness ratio of 48 and 33, respectively. These struts were annealed pin-ended specimens. Both coupon tests and monotonic/cyclic tests were conducted on full cross-sections of pipe to determine the material properties. The average yield strength of the annealed

material was 242 MPa and 214 MPa as measured from the coupon tests and from the full cross-section material tests, respectively.

As reported by the researchers, for strut 1 local buckling was observed at the mid-length during cycle 3. Local buckles tended to straighten out under tensile load, but reformed when compressive load was again applied. Tears developed in the steel during cycle 5 owing to the large local strain reversal associated with this behavior. For strut 2, a slight ovaling of the cross-section at the mid-length occurred during the fourth cycle. Local buckling developed in this region during the fifth cycle and tearing of the steel initiated during cycle 8.

The detailed comparison of the finite element analysis results with the findings in this experimental study will be presented later as an individual part and several conclusions will be drawn.

1.2.1.3 Study of Tremblay (2002)

A review of 76 cyclic loading tests on bracing members from nine different test programs was carried out to recommend values for the seismic design of concentrically braced frames. Fracture of RHS (rectangular hollow section) bracing members was found to depend strongly upon the slenderness ratio of the bracing members and, to a lesser extent, on the width-to-thickness ratio of the cross-section and the imposed displacement history. Slender braces can sustain higher ductility levels prior to fracture. Since the strain demand in the plastic hinge reduces with the brace slenderness, slender braces were considered to sustain higher ductility levels prior to fracture. Therefore, the study has proposed that width-to-thickness ratios should be specified for less slender members and minimum brace slenderness should be prescribed to achieve a given ductility level.

1.2.1.4 Study of Lee, Bruneau (2005)

In this paper, the existing experimental data are reviewed to quantify the extent of hysteretic energy achieved by bracing members in compression in past tests, and the extent of degradation of the compression force upon repeated cycling loading. It was found that the normalized energy dissipation of braces having moderate *KL*/*r* (80–120) do not have significantly more normalized energy dissipation in compression than those having a slenderness in excess of 120. The normalized degradation of the compression force envelope depends on *KL*/*r* and is particularly severe for W-shaped braces.

1.2.1.5 Study of Lee, Liu (1987)

Lee and Liu (1987) has conducted tests on bracing members of square and rectangular tubular sections made of A500 grade B steel. The results have shown that fracture life of bracing members is very sensitive to width-thickness ratio of the compression flange of the sections. The fracture life is also dependent on slenderness ratio, width to thickness ratio and mechanical properties of steel. The study has revealed that the fractures in bracing members were caused by severe local buckling in the region of plastic hinges and it is a result of large deformation cycles (larger than yield displacement). Local buckling did not occur before overall buckling, overall buckling caused plastic hinges followed by local buckling. Therefore, the overall buckling also affects the fracture life of the bracing member. According to test results a larger slenderness ratio (*KL*/*r*) caused less severe local buckling. As a past referral, Jain and Goel (1978) has suggested that braces with slenderness ratio (*KL*/*r)* smaller than 60 could be considered as small and for that members slenderness has no effect in the fracture criterion.

1.2.2 Analytical Studies

Several analytical studies (Tang and Goel, 1989; Perotti and Scarlassara, 1991; Ikeda and Mahin, 1986) were carried out for the inelastic response of steel braces and braced frames of multistory buildings. Section shapes, material behavior, residual stresses, damage accumulation due to low-cycle fatigue and fracture were all taken into account in those analytical models. The results were compared for multiple-storey and one-storey systems, and several conclusions were drawn for the effect of section shape and loading history on brace fracture and dissipation of energy. All of these models are not suitable for capturing the local buckling response.

The comparison was also made with the phenomenological models and it was revealed that the phenomenological model needs sufficient experimental data to define the numerous input parameters required. Since this is not usually the case as the experimental data is limited, the physical theory model was expected to give more reliable results. On the other hand, the physical models were declared to require more computational effort than phenomenological model.

However, with the rapid increase in computing power, it is now possible to conduct detailed finite element simulations in a reasonable amount of time. In order to simulate local buckling, a detailed finite element analysis can be conducted.

1.3 Problem Statement

Width-thickness limits are usually developed based on the monotonic test results. Zayas et al. (1980) pointed out that American Petroleum Institute (API) criterion (API 1977), which forms the basis of current AISC limit (Eqn. 1.3), does not necessarily preclude local buckling of pipe section braces under severe cyclic loading. It is reasonable to question the accuracy of the *D/t* limits presented in

design specifications. Further, the target ductility of the members designed according to the provisions is unclear. The dependence of ductility levels on the prescribed limits become increasingly important in an era where members/structures are designed to meet certain performance objectives. In addition, width-thickness limits are not dependent on the slenderness of the members according to the current provisions. It has been recognized in the past (Tang and Goel 1989; Goel and Lee 1992) that the post-buckling cyclic fracture life of bracing members generally increases with an increase in slenderness ratio.

All of the above mentioned concerns presented the need to reevaluate the slenderness and width thickness limits. Pursuant to this goal a numerical study has been undertaken to investigate the behavior of pipe section steel braces under severe cyclic loading. Fifty-four pin ended braces with different slenderness and width-thickness ratios were analyzed using the finite element method. The importance of the hardening modulus on the response was explored.

To ensure the reliability of finite element analysis, comparison between finite element analysis and experimental studies will be presented. Details of the numerical study on 54 braces will be given. Dependence of local buckling on geometrical and material properties is discussed. Results are presented in terms of the ductility level attained by the members. Later, energy dissipation characteristics of the analyzed braces are examined.

Finally, the relationship between the slenderness ratio and energy dissipation is explored for various target ductility levels.

CHAPTER 2

FINITE ELEMENT ANALYSIS PROCEDURE AND VERIFICATION WITH EXPERIMENTAL FINDINGS

2.1 Finite Element Modeling and Simulation Details

In this study a commercially available finite element program ANSYS (2006) was used to conduct the analysis. Round HSS (hollow structural section) steel braces were modeled with 8-node shell elements (shell93). The element has six degrees of freedom at each node: translations in the global x, y, and z directions and rotations about the nodal x, y, and z axes. The element has plasticity, stress stiffening, large deflection and large strain capabilities. Quadratic interpolation is used in the formulation of this element. The element uses 4 integration points (2x2) in-plane and 5 integration points through the thickness. A three dimensional finite element mesh shown in Figure 2.1 was prepared for each analysis. Twenty and fifty shell elements were used around the circumference and along the half-length, respectively. Owing to the symmetry, only half of the brace along the length was modeled to reduce the computational cost. The symmetry of the problem can vanish after local buckling occurs if the buckling mode is unsymmetrical with respect to the original plane of symmetry. However, during experiments a local buckle which is symmetrical with respect to the plane of symmetry was observed (Zayas et al. (1980)). In addition, at early stages of research full-length models were analyzed and their results were compared with the results of half-length models. Comparisons reveal that for pin-ended braces a symmetrical local buckle occurs at the mid-length and the results for the full- and half-length models were identical. Based on these observations, half-length models were used for the rest of the simulations.

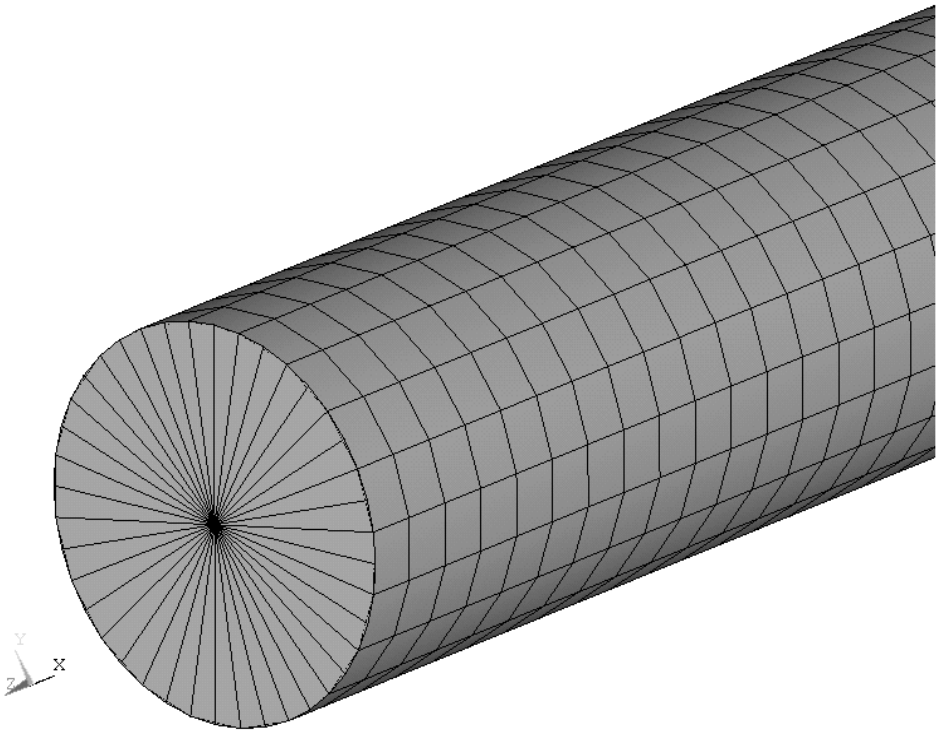

Figure 2.1 : Finite Element Mesh at the Cap Portion

For the finite element models used in this thesis, in order to simulate a pin-end condition a very stiff cap was modeled at the end section of the brace (Figure 2.1). This cap portion was modeled using 4-node elastic shell elements (shell63) which can degenerate into a 3-node shell element. Displacements were applied at the center node of the cap which remains elastic during the analysis. A symmetry boundary condition was applied at the mid-length. Translations in the axial direction and rotations around two of the global coordinate axes were restrained for all the nodes that lie on the plane of symmetry.

Initial imperfections of the brace resulted during fabrication or placing into the frame need to be introduced into the finite element model for analysis purposes. The initial geometry of the brace was input as a half sine-wave where

the maximum imperfection is at the mid-length. This imperfection was determined from the initial camber values reported for the specimens of Zayas et al. (1980) as 6.4 mm for strut 1 and 1.5 mm for strut 2. For the specimens strut 14, 15 and 16 of Black et al. (1980), initial camber was not quantified so an average value of 3 mm was used in analyses.

The non-linear stress-strain behavior of steel was modeled using von Mises yield criterion with kinematic hardening. This option assumes the total stress range is equal to twice the yield stress, so that the Bauschinger effect is included in the analysis. Bauschinger effect is a property of most metals that arises as plastic deformation of metal increases the yield strength for tension and decreases the yield strength for compression. For comparison purposes, the bilinear and the multilinear hardening models were considered. In both hardening models the initial elastic modulus was taken as 200 GPa. According to the experimental (Zayas et al. (1980)) cyclic stress-strain curve shown in Figure 2.2, the hardening modulus (E_h) was taken as 1.0 GPa for the bilinear hardening case and material was assumed to yield at 214 MPa. Similarly, multilinear kinematic hardening was defined by determining the locus of stress-strain points from the experimental values. In the multilinear hardening it was assumed that the material yields at 107 MPa, hardens with a decreasing tangent modulus and reaches to approximately twice the yield stress value with a final hardening modulus of 1.0 GPa. The cyclic stress-strain response obtained using bilinear and multilinear models are compared with experimental (Zayas et al. (1980)) observations in Figure 2.2. It is obvious that the multilinear model is better in capturing the Bauschinger effect when compared with the bilinear model. The multilinear model has drawbacks in terms of defining the first yield point in monotonic loading. According to this model, material yields at a lower stress than the first yield observed in experiments. However, this kind of modeling can be useful in the presence of residual stresses which cause early yielding. For the simulation of experimental study of Black et al. (1980), the hardening modulus was calculated from the monotonic stress-strain curves of test specimens provided in the report of

the study. For Strut 14 and Strut 15, the hardening modulus was found as 0.84GPa and for Strut 16, as 1GPa according to this calculation.

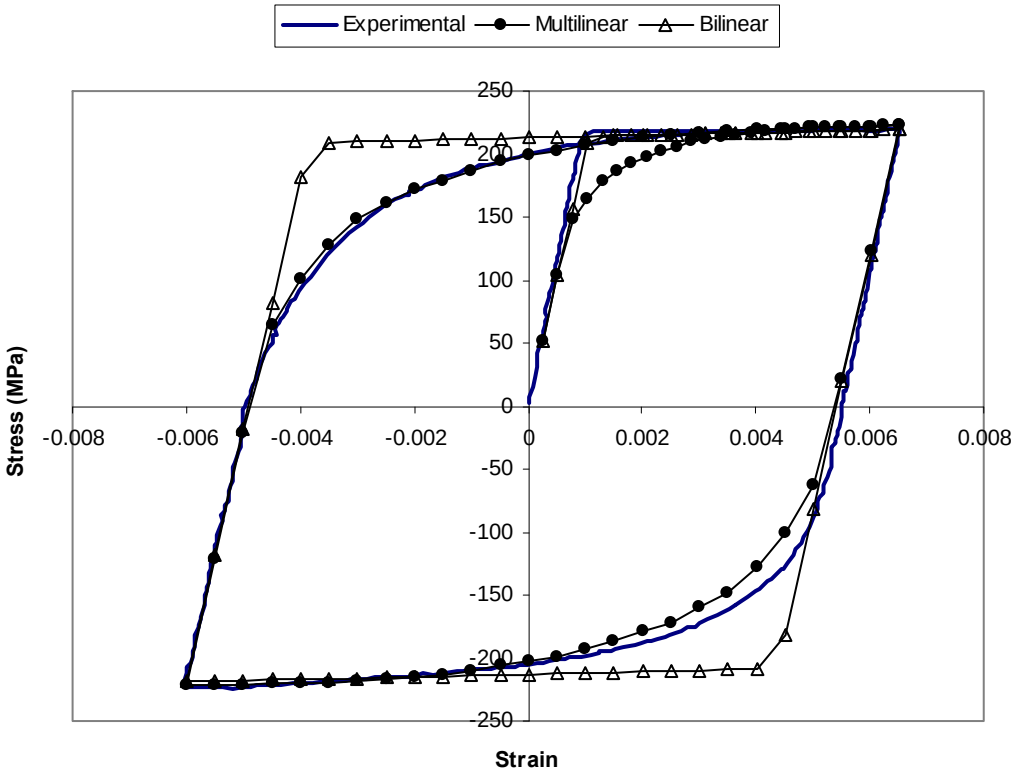

Figure 2.2 : Experimental (Zayas et al. 1980) and Numerical Cyclic Stress-Strain Curves

As indicated in Chapter 1, strut 15 of Black et al. (1980) was given an initial tension loading. For preliminary analyses, it was observed that the initial imperfections introduced into the model vanished when the member was initially subjected to tensile loading. When imperfections vanish, the member becomes perfectly straight and this has an adverse effect on the results. The straight member does not buckle in the subsequent cycles and this results in higher reaction forces forming under compressive loading. In order to eliminate this undesirable behavior, a tension-only link element (link10) was added to the finite element model as shown in Figure 2.3. The tension-only link was connected to

the uppermost node of the cross-section which lies on the plane of symmetry. The other end of the link was connected to a fixed support. The 750mm long link provides no resistance when the member buckles. However, when the member is subjected to tensile forces, the link element prevents the straightening of the member and ensures that the amount of initial imperfection is maintained in between the loading cycles.

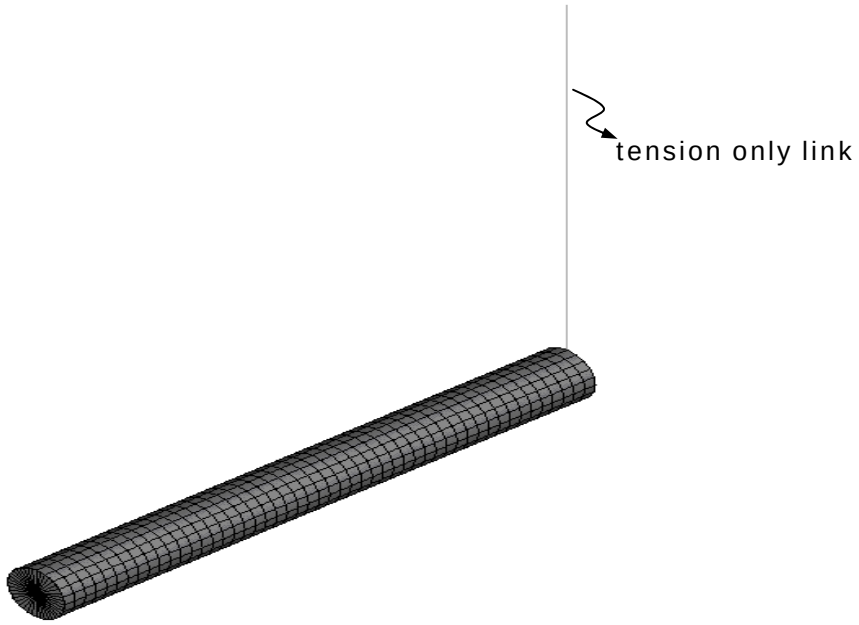

Figure 2.3 : 750 mm long tension-only link

In all analyses a displacement history was applied to the center node according to the value of displacements attained during experiments. The entire non-linear load-displacement history was traced using Newton-Raphson method. In all analyses geometrical and material nonlinearities were included. During a typical analysis, axial displacements, axial forces, lateral displacements at mid-length and plastic strains at certain nodes were recorded. Plastic strains in the axial direction were obtained for 10 nodes located on the top and for 10 nodes located on the bottom surfaces of the brace. These nodes were located on cross sections that are nearest to the plane of symmetry.

2.2 Comparison of Finite Element Analysis Results with Experimental Findings

As briefly described in Chapter 1, two experimental surveys, Zayas et al. (1980) and Black et al. (1980), were used as reference for the verification of finite element study performed in this thesis. Finite element analyses were conducted to simulate the behavior of the pipe specimens Strut 1 and Strut 2 of Zayas et al. (1980) and Strut 14, 15, and 16 of Black et al. (1980) under cyclic loading.

For Strut 1 and Strut 2 of Zayas et al. (1980), bilinear kinematic and multilinear kinematic hardening were used independently in the analyses. The global axial load versus displacement response of both struts is presented in Figure 2.4. In this figure first five cycles of the experimental findings of Zayas et al. (1980) are compared against the finite element simulations using two different material hardening laws. Comparisons reveal that finite element simulations are in good agreement with the experimental observations. Models with different hardening laws produced slightly different results.

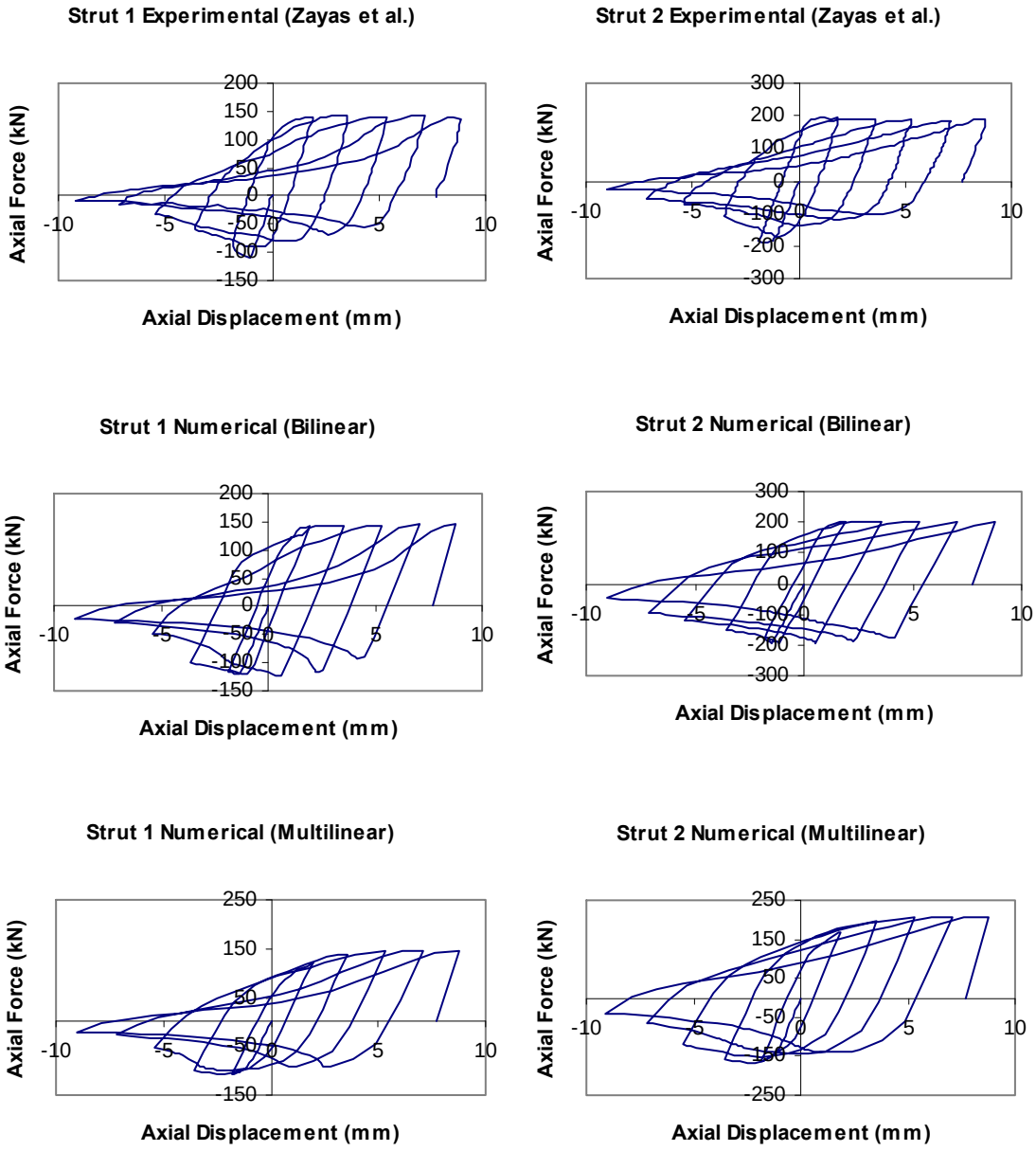

Figure 2.4 : Comparison of Experimental Findings with Numerical Simulations

In order to gain a better understanding of the simulation capabilities, a detailed investigation was conducted. Particularly, the maximum compressive and tensile loads, and energy dissipation at each cycle were considered. In Table 2.1 the maximum compressive and tensile loads and energy dissipation for each cycle as reported by Zayas et al. (1980) are given. For comparison purposes the maximum compressive and tensile axial loads and energy dissipation at each cycle were obtained from the finite element analysis results. Findings from the finite element analysis are normalized with the experimental results and are presented in Table 2.1. Comparisons are provided for analyses with different material modeling assumptions.

For both struts the maximum tensile loads at each cycle are well predicted. In general, the over-prediction of tensile loads is lower for the models with multilinear hardening as compared to the models with bilinear hardening. If average value of tensile loads in five cycles is considered, the maximum amount of over-prediction is 9% and is observed for Strut 1 modeled with bilinear hardening. Over-predictions of the tensile loads, in general, can be attributed to the higher yield strength possessed by the specimens. As mentioned before, yield strength values from coupon tests were higher than the ones from the full cross-section tests.

The maximum compressive loads are not well predicted when compared with the predictions of tensile loads. Experimental results show that the maximum compressive load decreases significantly with each subsequent loading cycle. This decrease is highly dependent on the presence of the Bauschinger effect and on the amount of imperfections. The maximum compressive load for early cycles is predicted better when compared to the later cycles. Obviously, the use of multilinear kinematic hardening in modeling improves the predictions. The amount of average over-prediction reduces from 40% to 23% and from 24% to 2% for struts 1 and 2, respectively with the use of multilinear hardening as opposed to bilinear hardening.

Table 2.1: Comparison of Finite Element Analysis Results with Experimental Findings

STRUT 1												
Experimental						Numerical						
						Bilinear Hardening			Multilinear Hardening			
Cycle Number	Displacement (mm)		Load (kN)		Energy Dissipation (kN-mm)	Normalized Load		Normalized Energy Dissipation	Normalized Load		Normalized Energy Dissipation
	Compression	Tension	Compression	Tension		Compression	Tension		Compression	Tension	
1	-1.829	1.930	102.3	124.5	335.6	1.13	1.13	0.56	1.04	0.97	0.55
2	-3.607	3.581	95.6	134.8	844.1	1.27	1.07	1.02	1.11	1.03	0.89
3	-5.385	5.334	86.7	133.4	1204.6	1.43	1.08	1.00	1.13	1.08	1.07
4	-7.163	7.087	72.1	133.9	1109.7	1.63	1.08	1.02	1.31	1.10	1.15
5	-9.042	8.788	61.4	132.6	1182.0	1.54	1.09	1.10	1.56	1.11	1.12
Average						1.40	1.09	0.94	1.23	1.06	0.96
Standard Deviation						0.20	0.03	0.22	0.21	0.06	0.25

STRUT 2												
Experimental						Numerical						
						Bilinear Hardening			Multilinear Hardening			
Cycle Number	Displacement (mm)		Load (kN)		Energy Dissipation (kN-mm)	Normalized Load		Normalized Energy Dissipation	Normalized Load		Normalized Energy Dissipation
	Compression	Tension	Compression	Tension		Compression	Tension		Compression	Tension	
1	-1.854	1.880	194.4	198.8	452.0	0.90	1.01	0.58	0.80	0.85	0.57
2	-3.556	3.581	177.9	195.7	1350.4	1.01	1.04	0.88	0.87	1.00	0.79
3	-5.486	5.309	139.2	195.7	1735.7	1.30	1.04	1.15	1.02	1.05	1.12
4	-7.163	7.061	122.3	191.7	2021.6	1.43	1.06	1.27	1.11	1.08	1.12
5	-9.068	8.763	104.5	191.3	1957.2	1.59	1.07	1.19	1.29	1.09	1.20
Average						1.24	1.04	1.01	1.02	1.01	0.96
Standard Deviation						0.29	0.02	0.28	0.19	0.10	0.27

The energy dissipation at each cycle is well predicted except the first cycle. The use of both the bilinear and the multilinear kinematic hardening models is not sufficient to predict the energy dissipated in the first cycle. When this loading cycle was examined closely, it was observed that there are discrepancies in the load-displacement behavior especially for the region that starts with the maximum compressive displacement and ends with the maximum tensile displacement. However, large discrepancies that occur during the first cycle are not significant when cumulative energy dissipation is concerned. The amount of energy dissipated in the first cycle is much less compared to the energy dissipated in subsequent cycles. Both the bilinear and the multilinear kinematic models are sufficient to capture the energy dissipation for cycles after the first cycle.

An appropriate criterion needs to be selected for tracing the formation of local buckling. It is hard to discern from the deformed finite element mesh whether local buckling has initiated or not. Local buckling can be observed from the deformed shape a few cycles after its initiation as shown in Figure 2.5.

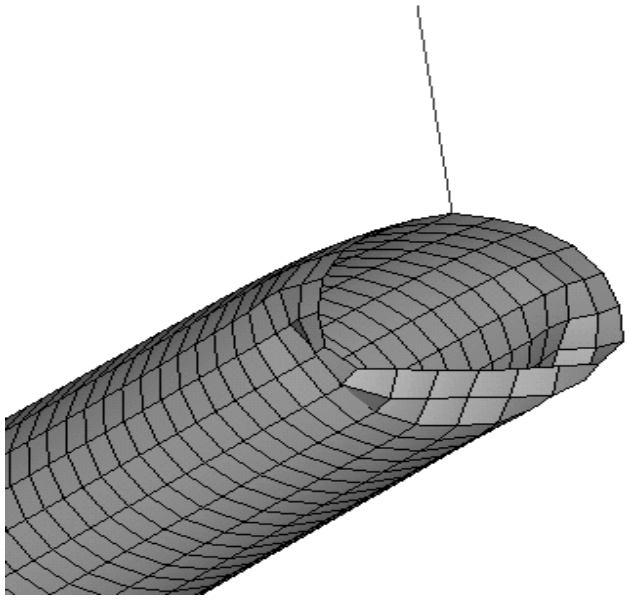

Figure 2.5 : Local buckling in the finite element model

A criterion based on local strain measures is adopted in this study. Basically the plastic strain in the longitudinal direction of the braces was traced at two nodes. These nodes, hereafter referred as node 1 and node 2, lie on the bottommost point of the cross section. Node 1 is located on a cross section which lies on the plane of symmetry, whereas node 2 lies on a cross section which is one-element away from the plane of symmetry as shown in Figure 2.6. Variation of plastic strains at two nodes obtained from the finite element analysis utilizing multilinear and bilinear hardening are given in Figure 2.7 for struts 1 and 2.

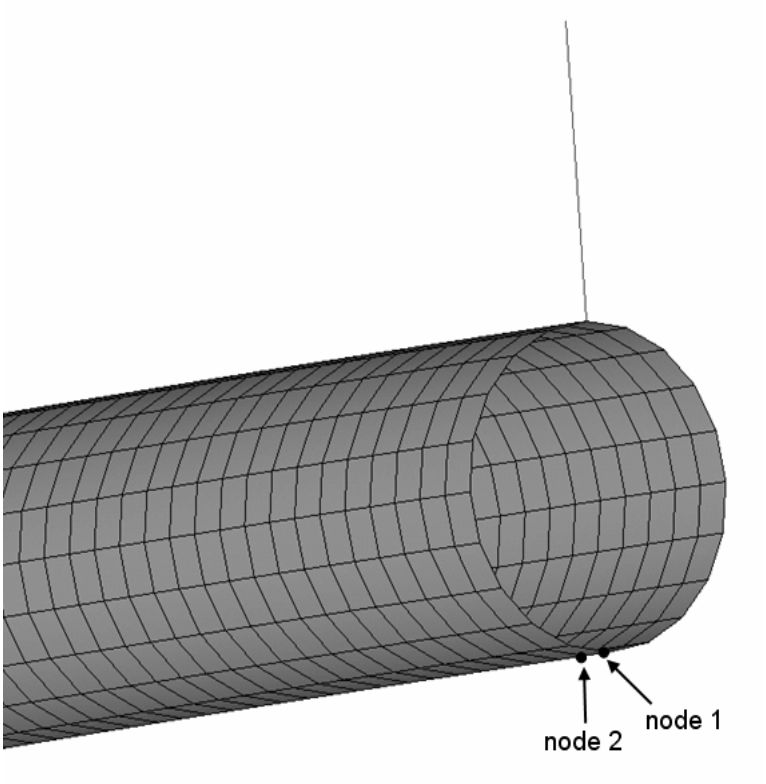

Figure 2.6 : Locations of node 1 & 2

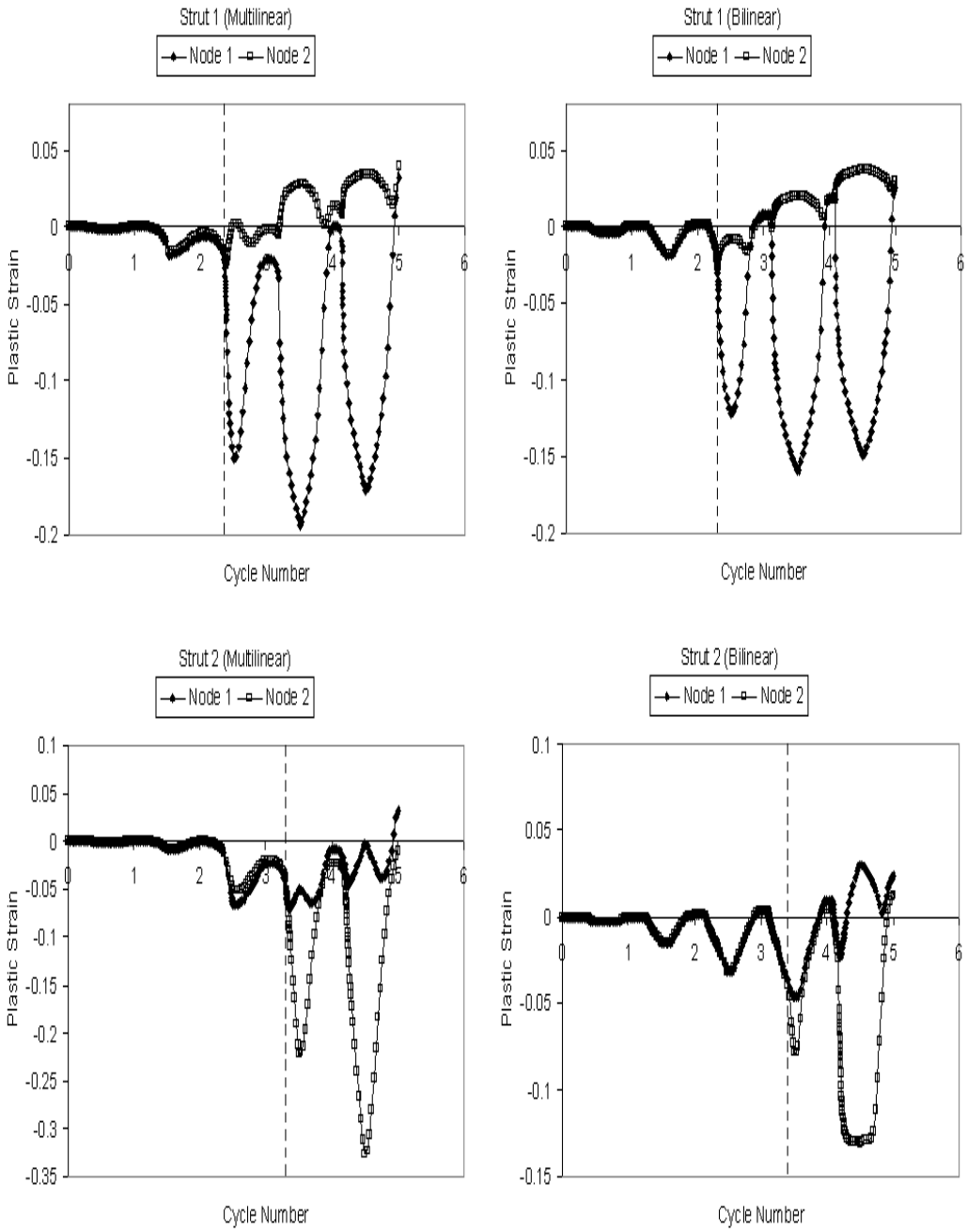

Figure 2.7 : Variation of Plastic Strains

It is clear from these figures that both nodes experience the same amount of plastic strain until the end of cycle number 2 and cycle number 3 for struts 1 and 2, respectively. Following these cycles a significant difference between the plastic strain values are observed. The displacement value at which the plastic strains start to deviate from each other is considered as the local buckling initiation point in this study. According to this criterion, strut 1 buckles after cycle number 2 during the compressive excursion of cycle number 3. This observation is conformable with the experimental observations. Similarly, strut 2 buckles after cycle number 3 during the compression excursion of cycle number 4. This observation is slightly different than the reported one where buckling was observed in cycle number 5. However, as mentioned before, ovaling of the cross-section was observed in the experiment at cycle number 4. The deviation of plastic strains in cycle number 4 can be an indication of the ovaling of the cross-section, therefore the initiation of local buckling. Similar conclusions can be drawn if analysis results with bilinear hardening are considered (Figure 2.6). Although the local strain values differ between the two models with different material hardening laws, the initiation point of local buckles are the same for both cases.

Also, struts 14, 15 and 16 of Black et al. (1980) study were simulated using the finite element methodology employed herein. Severe local buckling was not reported for these struts. Therefore, the load-displacement responses obtained from the simulations were compared with the experimental observations. The axial load versus displacement response of these three struts is presented in Figure 2.8. In this figure, experimental findings Black et al. (1980) are compared against the finite element simulations as both plotted on the same graph for the ease of comparison. The unlined dots are the experimental data points and the lines represent the finite element results.

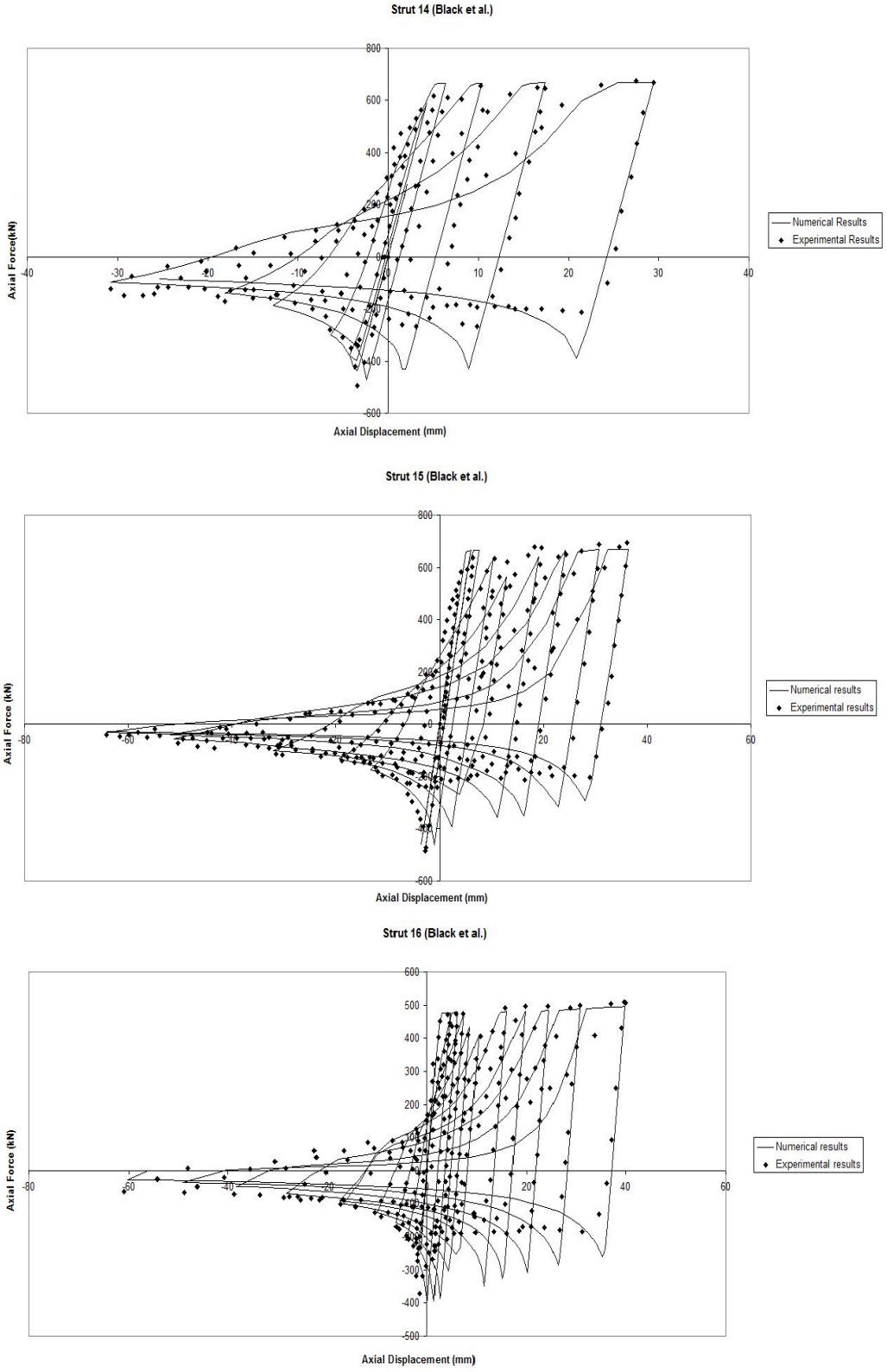

Figure 2.8 : Comparative load-displacement curves for Strut 14-15-16

As can be seen from this figure, similar conclusions related with strut 1 and 2 can be drawn for struts 14, 15, and 16 in terms of the load-displacement behavior. The maximum tensile loads were better predicted than compressive loads as Bauschinger effect and the amount of initial imperfection affects the peak compressive loads during cyclic loading. Besides, for the post-buckling behavior finite element simulation fits satisfactorily with the experimental results.

CHAPTER 3

PARAMETRIC FINITE ELEMENT STUDY OF ROUND HSS SEISMIC BRACING

3.1 Details of the Parametric Study

After the verification of finite element model with the experimental findings for which the details are given in Chapter 2, a parametric study has been conducted on round HSS (Hollow Structural Section) seismic bracing using this finite element methodology. The aim of this parametric study is to investigate the effect of several parameters such as slenderness ratio, diameter-to-thickness ratio, hardening modulus on the initiation of local buckling and the amount of energy dissipated through inelastic displacements.

All the braces in this study are pinned at both ends and slenderness values of 40, 60, 80, 100, 120, 140, 160, 180, and 200 were considered. For each slenderness value, diameter-to-thickness ratios of 5, 10, 15, 20, 25, and 30 were considered. For the selection of these values, provided limits in the current specifications (AISC Seismic Provisions 2005, Eurocode 3) were used. According to the formulas specified in Chapter 1, for the AISC Seismic Provisions (2005) and the Eurocode 3 (2003), diameter-to-thickness limits for compactness are 29.3 and 39.3, respectively for a round HSS with 300 MPa yield. In this study, a total of 54 pin-ended braces were analyzed. In all analyses the yield strength and the length of the brace member were taken as 300 MPa and 4500 mm, respectively. A displacement based loading protocol given in Figure 3.1 was applied in all analyses. In this loading protocol, braces were subjected to hysteretic tension-compression loading with increasing axial displacements after each cycle. All braces were subjected to displacements ranging from 1 to 10 times the yield displacement (Δ_y) of the brace in tension.

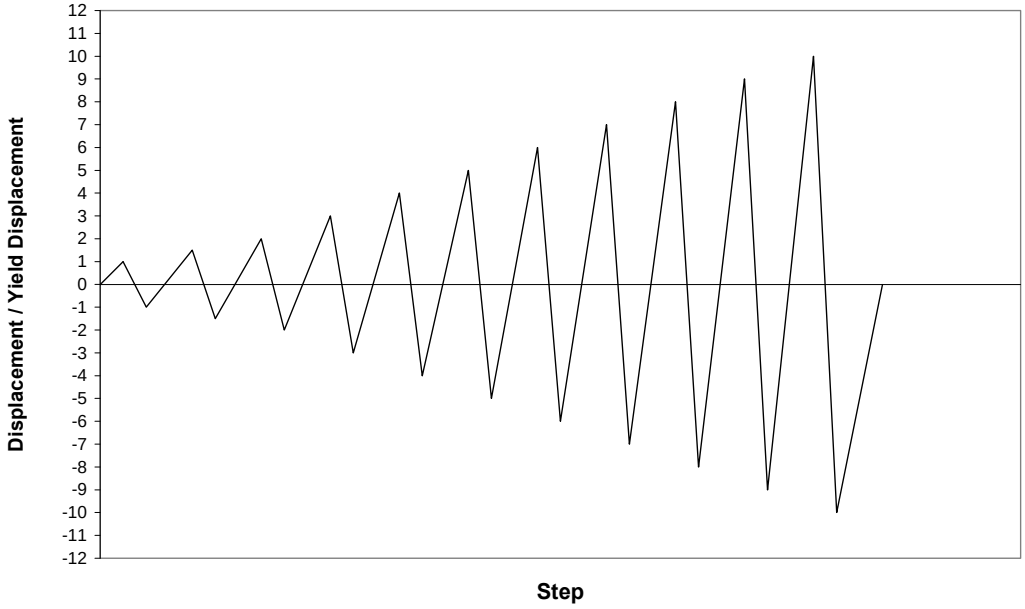

Figure 3.1 : Loading Protocol

Furthermore, the effect of cyclic hardening modulus on the response of braces was explored. In the past researches, it was found that the mechanical behavior of the material under cyclic loading is much more complicated than that of monotonic loading. A representative cyclic stress-strain curve obtained by Cofie and Krawinkler (1985) is given in Figure 3.2. As can be seen from this figure, the nonlinear portions of the stress-strain curve can be defined by continuously changing tangent modulus whose magnitude is a function of the distance between a stress bound and the instantaneous stress. The presence of these bounds was proposed by Dafalias and Popov (1975) in formulating bounding surface plasticity. At large inelastic strains, a rate of decrease in stiffness approaches zero as shown in Figure 3.2 and the stress-strain curve approaches a straight line bound. The slope of the stress bound is not unique like the elastic modulus but is dependent on the type and the fabrication of steel.

Cofie and Krawinkler (1985) reported that the slope of stress bound is equal to E/134 for A36 specimen experimented in their study. Shen et al. (1995) reported values of E/111, E/71, and E/200 for Japanese steels SS400, SM490, and SM570, respectively. Usami and others (2000) observed that the slope of stress bound is not a constant and becomes very small when material experiences large plastic deformation. In the refined plasticity models by Usami and others (2000) the slope of the stress bound was assumed to decrease with the amount of plastic work.

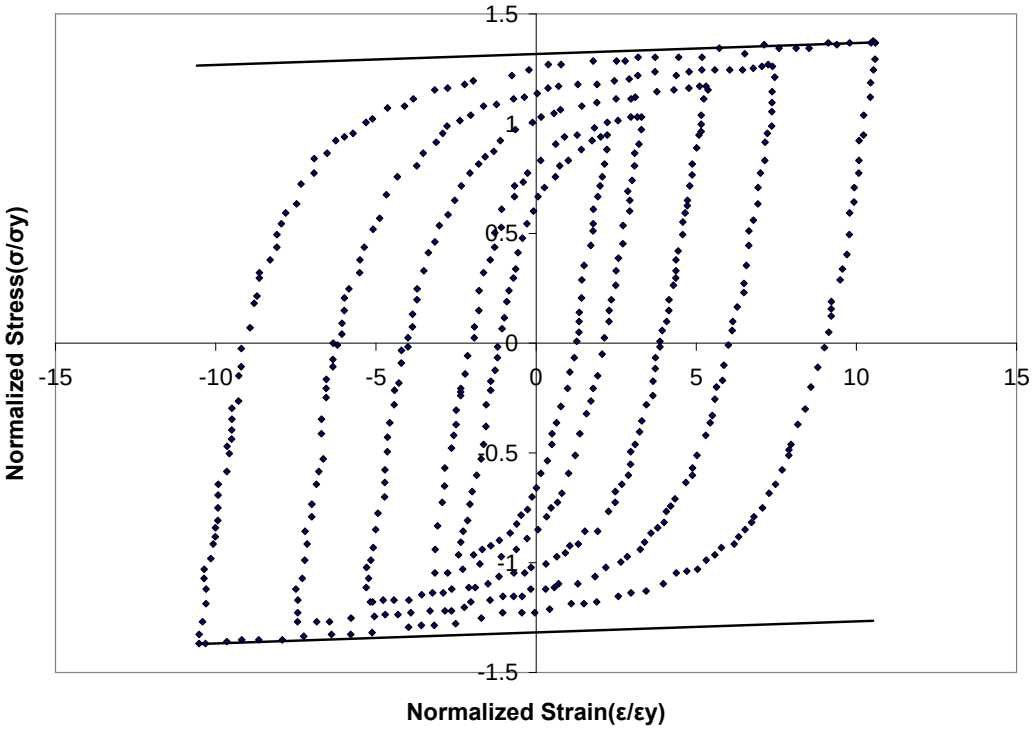

Figure 3.2 : Cyclic Stress-Strain Curve from Cofie and Krawinkler (1985) and the Stress Bounds

Based on the review of previous work on material behavior, the cyclic hardening modulus was considered as a variable in the parametric study. In all analyses bilinear kinematic hardening was used and the hardening modulus (E_h)

beyond the yield point was changed. Particularly, hardening modulus values of 1 GPa (E/200), 2 GPa (E/100), 4 GPa (E/50), and 8 GPa (E/25) were considered. All 54 braces were analyzed under different hardening modulus assumptions resulting in a total of 216 runs.

3.2 Results of the Parametric Study

3.2.1 Local Buckling

Local buckling was traced using the local strain criterion that was explained in Chapter 2. For all analyses the plastic strain after the compression portion of each cycle was plotted for two neighboring nodes (nodes 1 and 2). The local buckling was assumed to initiate at the cycle where significant deviation between plastic strains occur. A representative plot is given in Figure 3.3. In this figure, comparative plastic strains of node 1 and 2 for the brace that has D/t=15, slenderness (KL/r) of 100 and hardening modulus of 2GPa is presented. As it can be seen from the figure, deviation of plastic strain for the consecutive nodes begins at almost twentieth cycle. According to the loading protocol given in Figure 3.1., this cycle corresponds to a ductility level of $-5\Delta_y$. Therefore, the initiation of local buckling is considered as $5\Delta_y$ for this case. According to this criterion the initiation of local buckling as a function of the yield displacement (Δ_y) was determined and these results are presented in Table 3.1. In this table empty cells represent the cases where no local buckling was observed. For the rest of the cases the ductility level at which the local buckling initiates is reported.

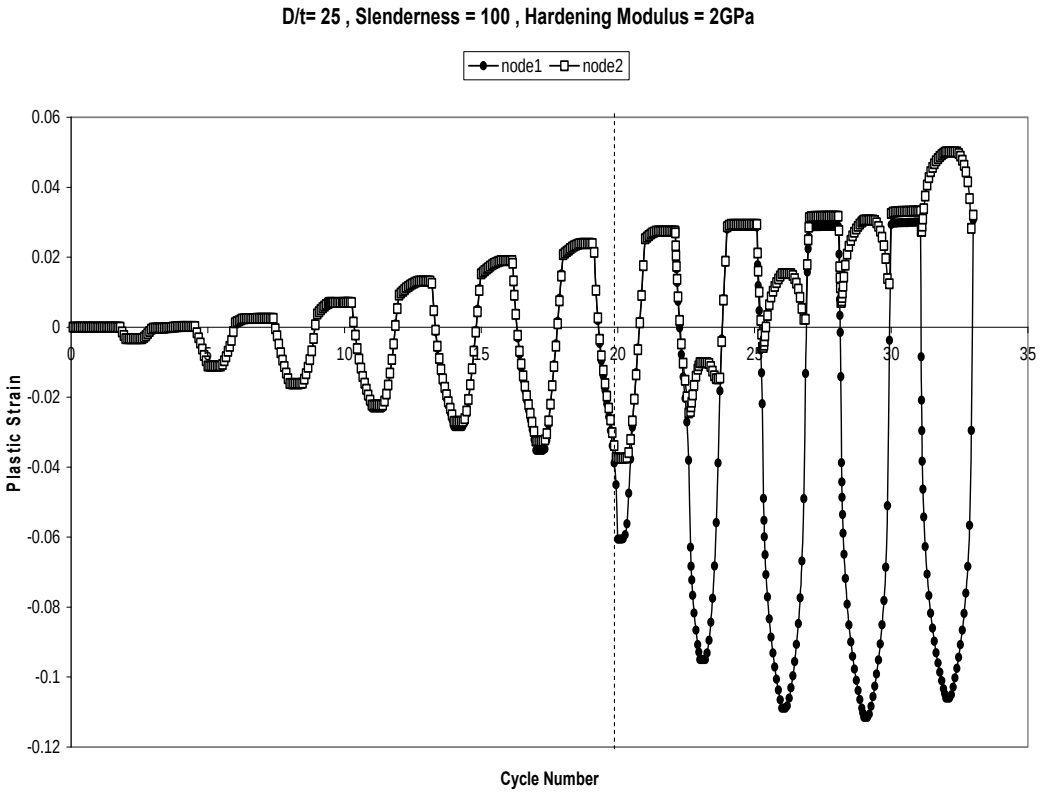

Figure 3.3 : Local Buckling Criterion Using Plastic Strains

According to the numerical findings, the local buckling is significantly influenced by the cyclic hardening modulus adopted. Among the braces with 8 GPa (E/25) hardening modulus, only one exhibit local buckling while 29 braces, with 1 GPa (E/200) hardening modulus, buckle locally. In addition, cyclic hardening modulus has a positive effect on increasing the ductility level at the onset of local buckling. For a particular slenderness and diameter-to-thickness ratio, the ductility level reached at local buckling increases as the hardening modulus increases. Diameter-to-thickness limits in code provisions depend on the elastic modulus and the yield strength. Numerical findings reveal that these limits should also be dependent on the cyclic hardening modulus of the steel used.

Table 3.1.: Analysis Results for Local Buckling

Initiation of Local Buckling									
Hardening Modulus = 8 GPa (E/25)									
	Slenderness (KL/r)								
D/t	40	60	80	100	120	140	160	180	200
5									
10									
15									
20									
25									
30	$8\Delta_y$								
Hardening Modulus = 4 GPa (E/50)									
	Slenderness (KL/r)								
D/t	40	60	80	100	120	140	160	180	200
5									
10									
15									
20									
25	$7\Delta_y$	$9\Delta_y$							
30	$5\Delta_y$	$5\Delta_y$	$6\Delta_y$	$9\Delta_y$					
Hardening Modulus = 2 GPa (E/100)									
	Slenderness (KL/r)								
D/t	40	60	80	100	120	140	160	180	200
5									
10									
15									
20	$6\Delta_y$	$7\Delta_y$	$8\Delta_y$						
25	$5\Delta_y$	$5\Delta_y$	$5\Delta_y$	$5\Delta_y$	$6\Delta_y$	$7\Delta_y$	$8\Delta_y$		
30	$3\Delta_y$	$3\Delta_y$	$3\Delta_y$	$3\Delta_y$	$4\Delta_y$	$4\Delta_y$	$5\Delta_y$	$6\Delta_y$	
Hardening Modulus = 1 GPa (E/200)									
	Slenderness (KL/r)								
D/t	40	60	80	100	120	140	160	180	200
5									
10									
15	$7\Delta_y$	$8\Delta_y$	$9\Delta_y$						
20	$3\Delta_y$	$4\Delta_y$	$5\Delta_y$	$5\Delta_y$	$5\Delta_y$	$6\Delta_y$	$6\Delta_y$	$6\Delta_y$	
25	$4\Delta_y$	$4\Delta_y$	$4\Delta_y$	$4\Delta_y$	$5\Delta_y$	$5\Delta_y$	$6\Delta_y$	$6\Delta_y$	$6\Delta_y$
30	$2\Delta_y$	$2\Delta_y$	$2\Delta_y$	$2\Delta_y$	$3\Delta_y$	$3\Delta_y$	$4\Delta_y$	$4\Delta_y$	$4\Delta_y$

3.2.2 Energy Dissipation

As previously described in Chapter 1, bracing systems dissipate energy throughout inelastic cyclic displacements. The amount of energy dissipated by brace is vital during a severe seismic action. In this study, the hysteretic energy dissipated at each cycle was quantified based on the finite element analysis results. In order to provide a fair comparison between the braces, the hysteretic energy was normalized by the hysteretic energy dissipated if the strut was a buckling restrained brace. This approach can be illustrated in Figure 3.4. As it can be seen from the figure, the hysteretic energy dissipated by an elastic perfectly plastic system, which is equal to the area enclosed by the dashed lines, was considered for each individual cycle.

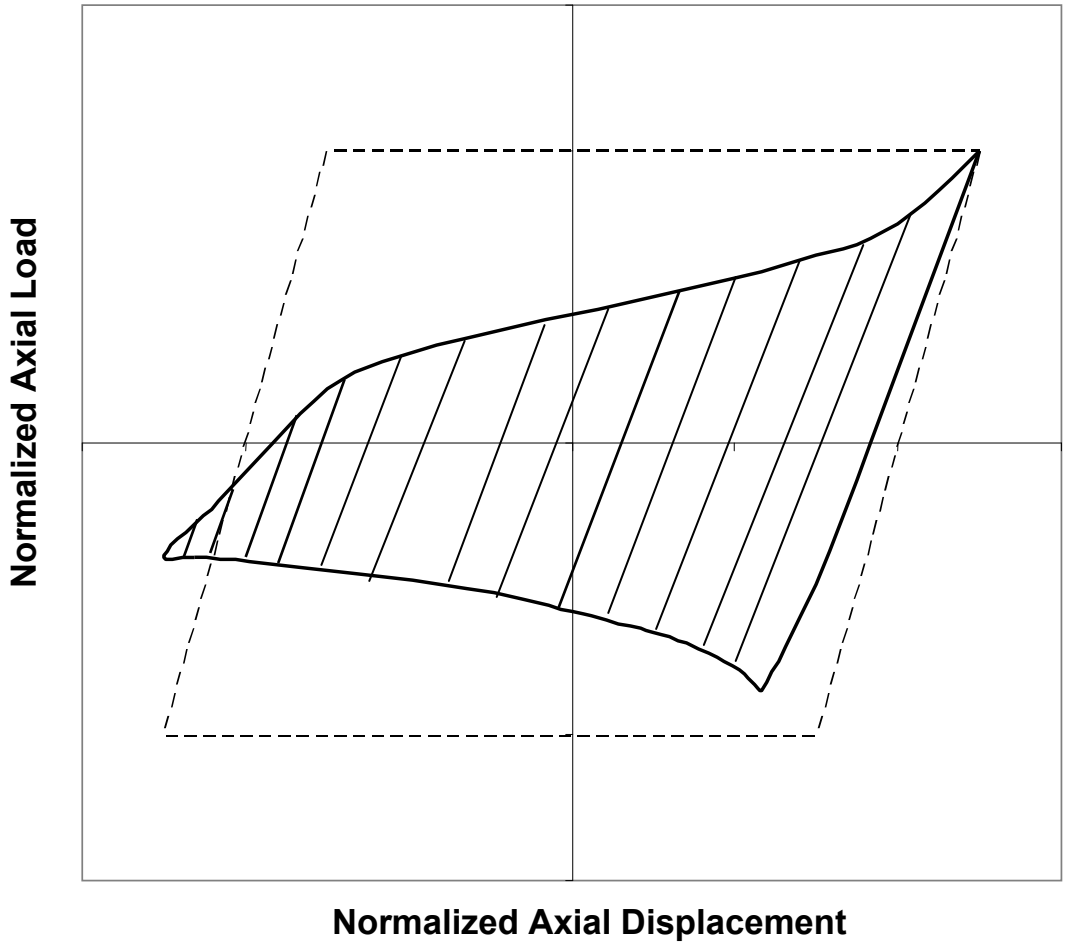

Figure 3.4 : Quantifying energy dissipation

The amount of energy dissipation is dependent on the ductility level at each cycle, the slenderness ratio, the diameter-to-thickness ratio and the cyclic hardening modulus adopted for the analysis. According to the results obtained from the analyses, the following general observations can be made.

Among many variables, the amount of energy dissipation is mostly influenced by the slenderness of the member and the ductility level at each cycle. Figure 3.5 shows a representative variation of the normalized energy dissipation as a function of the ductility level at each cycle for different slenderness ratios. It is evident from this figure that, for all slenderness ratios, normalized energy dissipation tends to decrease as the ductility level at any given cycle increases. Stocky braces dissipate much more energy as compared to slender braces at early cycles where the maximum displacement is less than or equal to twice the yield displacement. For displacement cycles greater than twice the yield displacement, normalized energies are almost constant for each of the slenderness values.

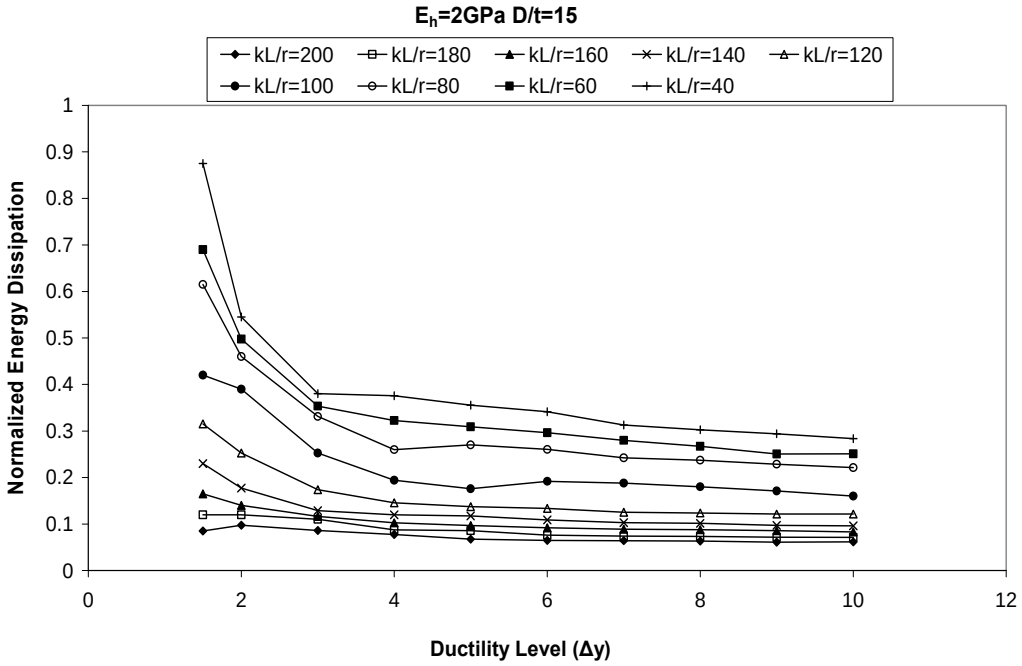

Figure 3.5 : Variation of Normalized Energy Dissipation for Various Slenderness Ratios

Analysis results reveal that for any given slenderness ratio and cyclic hardening modulus, the normalized energy dissipation is not significantly influenced by the diameter-to-thickness ratio. Figure 3.6 shows a representative variation of the normalized energy dissipation as a function of the ductility level at each cycle for constant slenderness of 100 and different diameter to thickness ratios. As can be seen from the figure, for compact sections with lower diameter to thickness ratios, amount of energy dissipation is relatively larger than the non-compact sections mainly for higher ductility levels. For early cycles where the ductility levels are smaller, the amount of energy dissipation is converging to the same level which is considerably higher than the level attained at the end of the analyses. Whereas, this trend is prevailing for stocky to moderate braces for which the slenderness ratios are relatively lower. As the slenderness increases larger energy dissipation at the early cycles of analyses is not apparent. In these slender braces, same degree of dissipated energy is preserved throughout the whole loading history and this level appears to be much lower than the higher ductility capacities of stocky braces. This finding is presented in Figure 3.7. In this figure, the normalized energy dissipation as a function of the ductility level for stocky braces (KL/r=40) and slender braces (KL/r=200) with different diameter-to-thickness ratios is plotted.

Among all the parameters concerned in this study, the least significant parameter for energy dissipation is the hardening modulus. The analysis results show that minor changes occur in the normalized energies for different hardening modulus and the amount of this difference increases slightly with increasing ductility levels. Figure 3.8 shows a representative variation of the normalized energy dissipation as a function of the ductility level for constant slenderness of 120 and diameter to thickness ratio of 10 and different hardening modulus.

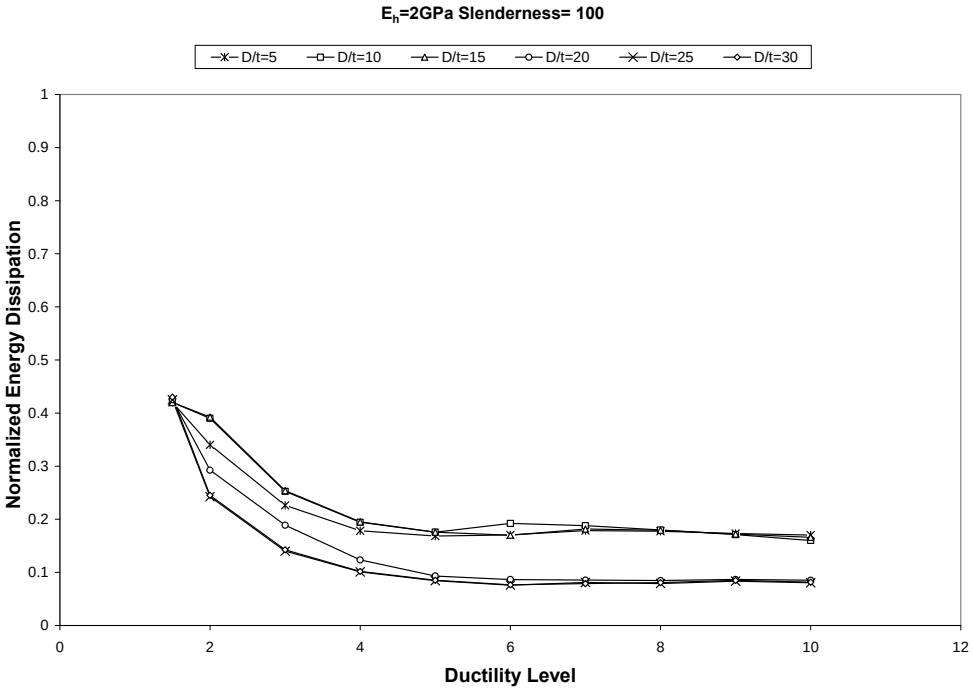

Figure 3.6 : Variation of Normalized Energy Dissipation for Various Diameter-to-Thickness Ratios

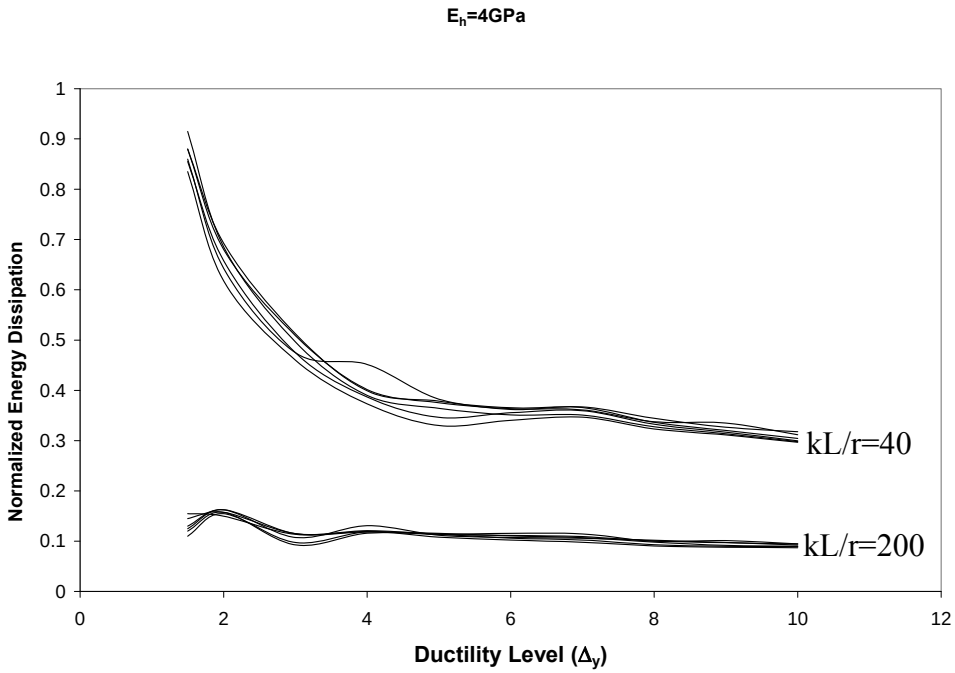

Figure 3.7: Comparison of Normalized Energy Dissipation for Stocky and Slender Braces with Different D/t Ratios

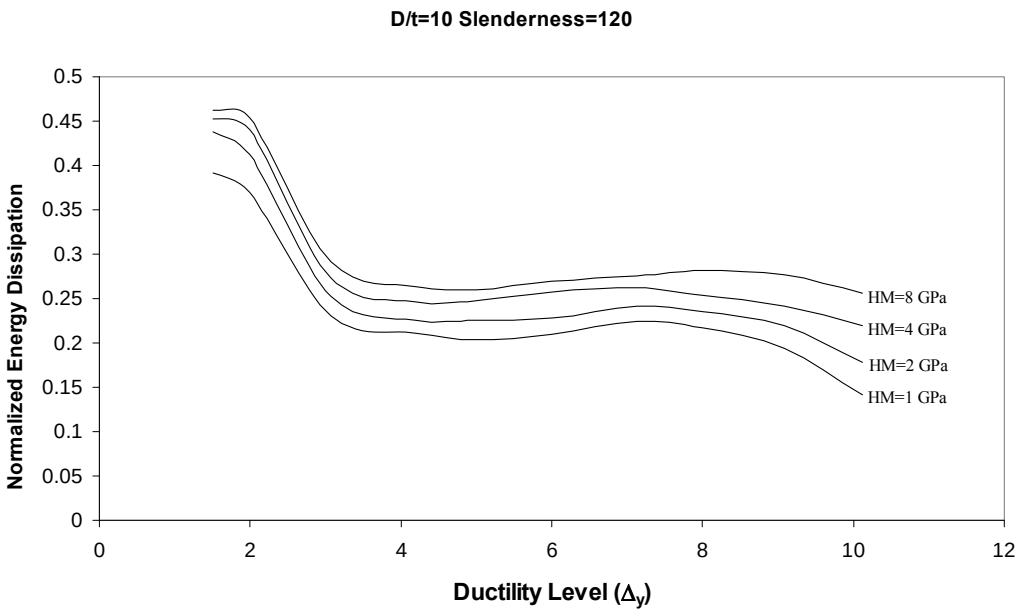

Figure 3.8 : Variation of Normalized Energy Dissipation for Various Hardening Modulus

CHAPTER 4

SUMMARY AND CONCLUSIONS

4.1 Summary

Seismic provisions for steel buildings present limiting width-thickness and slenderness ratios for bracing members. Most of these limits were established based on experimental observations. These experiments are very valuable but the amount of such studies is limited due to the costs associated with them. With the rapid increase in computing power, it is now possible to simulate the behavior of braces with finite element analysis by using personal computers and in a reasonable amount of time. In this thesis, a numerical parametric study has been conducted to investigate local buckling and energy dissipation of round HSS (Hollow Structural Section) seismic bracing.

In this study, finite element method is employed to examine the behavior of the structural members subjected to hysteretic tension-compression loading. Finite element methodology used in this study is described in Chapter 2. For the verification of the finite element model, experimental studies of Zayas et al. (1980) and Black et al. (1984) are considered as benchmarks. Two struts (strut 1 and 2) of Zayas et al. (1980) and three struts (strut 14,15 and 16) of Black et al. (1980) were modeled and analyzed with finite element method. All of these specimens are pipe section steel braces that are pinned at both ends.

In Chapter 3, a parametric study on 54 braces resulting in a total 216 runs has been conducted. Effects of certain parameters such as slenderness, diameter to thickness ratio, and hardening modulus on local buckling and energy dissipation of braces were investigated and defined.

4.2 Conclusions

The following conclusions were drawn based on the results of the study:

- When compared with the experimental findings, finite element simulations provide solutions with acceptable accuracy. With this simulation capability, response of brace members can be studied with less cost.

- Finite element analysis predictions are good for tracing local buckling and quantifying hysteretic energy dissipated by the brace member. On the other hand, predictions are not reliable for estimating the maximum compressive load at each cycle. Finite element methodology presented in this thesis needs to be refined to better predict the compressive loads.

- Results of the parametric study reveal that the local buckling is significantly influenced by the cyclic hardening modulus of the material. Members with low hardening modulus suffer local buckling at low ductility levels. In addition, members with high slenderness ratio are less susceptible to local buckling. Results presented in Table 3.1 can be used to determine the ductility levels at the onset of local buckling.

- Hysteretic energy dissipation at each cycle was found to depend on the level of ductility and on the slenderness ratio of the member. Braces with low slenderness ratio have higher normalized energy dissipation at early cycles when compared to braces with high slenderness. The difference between stocky and slender braces becomes less for displacement cycles that produce ductility levels in excess of two.

REFERENCES

- **AISC. 2005.** Seismic Provisions for Structural Steel Buildings. Chicago, Illinois.

- **American Petroleum Institute (API). 1977.** Recommended practice for planning, designing, and constructing offshore platforms. Dallas, Texas, Ninth Edition.

- **ANSYS 2006 Version 8.1** On-line User's Manual.

- **Black RG, Wenger WAB, Popov EP. 1980.** Inelastic buckling of steel struts under cyclic load reversals. Earthquake Engineering Research Center, Report No. UCB/EERC-80/40, University of California, Berkeley.

- **Cofie NG, Krawinkler H. 1985.** Uniaxial cyclic stress-strain behavior of structural steel. ASCE Journal of Engineering Mechanics, 111(9): 1105-1120.

- **Dafalias YF, Popov EP. 1975.** A model for nonlinearly hardening materials for complex loading. Acta Mechanica, 21: 173-192.

- **Dafalias YF, Popov EP. 1976.** Plastic internal variables formalism of cyclic plasticity. ASME Journal of Applied Mechanics, 43: 645-651.

- **Eurocode 3. 2003.** Design of steel structures. ENV 1993-1-1, Brussels, European Committee for Standardization (CEN).

- **Eurocode 8. 2003.** Design of structures for earthquake resistance. Part 1. Brussels, European Committee for Standardization (CEN).

- **Goel SC, Lee S. 1992.** A fracture criterion for concrete-filled tubular bracing members under cyclic loading. Proceedings of the 1992 ASCE Structures Congress, pp. 922-925.

- **Hassan O, Goel SC. 1991.** Seismic behavior and design of concentrically braced steel structures. Report UMCE 91-1, University of Michigan, Department of Civil and Environmental Engineering, Ann Arbor, MI.

- **Ikeda K, Mahin SA. 1986.** Cyclic response of steel braces. ASCE Journal of Structural Engineering, 112(2): 342-362.

- **Perotti F, Scarlassara P. 1991.** Concentrically braced steel frames under seismic actions: Non-linear behavior and design coefficients. Earthquake Engineering and Structural Dynamics, 20: 409-427.

- **Shen C, Tanaka Y, Mizuno E, Usami T. 1992.** A two-surface model for steels with yield plateau. Japan Society of Civil Engineers, Structural Engineering and Earthquake Engineering, 8(4): 179-188.

- **Shen C, Mamaghani IHP, Mizuno E, Usami T. 1995.** Cyclic behavior of structural steels II-theory. ASCE Journal of Engineering Mechanics, 121(11): 1165-1172.

- **Tang X, Goel SC. 1989.** Brace fractures and analysis of phase I structure. ASCE Journal of Structural Engineering, 115(8): 1960-1976.

- **Tremblay R. 2002.** Inelastic seismic response of steel bracing members. Journal of Constructional Steel Research, 58: 665-701.

- **Usami T, Gao S, Ge H. 2000.** Elastoplastic analysis of steel members and frames subjected to cyclic loading. Engineering Structures, 22: 135-145.

- **Zayas VA, Popov EP, Mahin SA. 1980.** Cyclic inelastic buckling of tubular steel braces. Earthquake Engineering Research Center, Report No. UCB/EERC-80/16, University of California, Berkeley.